arXiv:1703.05834v1 [cs.HC] 16 Mar 2017

Comprehensive Tracker Based Display Calibration for Holographic Optical See-Through Head-Mounted Display

Long Qian*
Johns Hopkins University
Baltimore, USA

Ehsan Azimi‡
Johns Hopkins University
Baltimore, USA

Peter Kazanzides§
Johns Hopkins University
Baltimore, USA

Nassir Navab¶
Johns Hopkins Univ., USA
TU München, Germany

Abstract

A holographic display system is able to offer an immersive 3D experience with a controllable focus cue that matches the depth information of virtual content. Proper calibration of an OST-HMD must take into account the specific features of that HMD. Existing calibration methods, however, cannot fully capture the optical characteristics of holographic display systems. With the aid of tracking systems, it is possible to register rendered graphics with tracked objects in the real world, providing an augmented reality experience for the users. We propose a new calibration procedure to properly align the coordinate system of rendering with that of the tracker. In this paper, both internal and external tracking systems are studied; three models of the mapping from tracking space to display space are presented: isometric, affine and perspective transformation. Experimental results demonstrate the validity of our method. Additionally, in a novel approach, the implementation uses self localization and spatial mapping of the HMD with an external tracker to perform this calibration, eliminating the requirement for line of sight from the HMD to the object or tracker. Microsoft HoloLens is used as the holographic OST-HMD for our experiments. The experimental results indicate an accuracy of up to 4 mm in the average reprojection error for the general perspective case and similarly 4 mm in our objective evaluation. To the best of our knowledge, this is the first OST-HMD calibration method that takes the holographic nature of the display technology into account.

Index Terms: H.5.1 [Information Interfaces and Presentation]: Multimedia Information Systems—Artificial, augmented, and virtual realities; I.4.3 [Image Processing and Computer Vision]: Enhancement—Geometric correction

1 Introduction

The use of optical see-through head-mounted displays (OST-HMD) for augmented reality applications has increased significantly in recent years, due to the engineering advances in commercial OST-HMD devices. One particular area that has remained challenging for these systems is the display calibration [17]. Since augmented reality has to visualize virtual objects in reality, the correct pose and proper alignment of the displayed object is of critical importance for the proper user experience using such systems, for example in surgical navigation [2, 25, 29]. The calibration procedure is aimed to compute the transformation so that the virtual objects to be augmented can be represented in the same coordinate system as the real world objects.

Many methods intend to improve the display calibration procedure in terms of accuracy [23, 30], robustness [3, 26, 27], and user-friendliness [15, 16]. However, the OST-HMDs being calibrated are either monoscopic or stereoscopic, based on the availability of OST-HMD display technology at the time. Most recently, holographic head-mounted displays such as HoloLens came into the market with some unique features and optical characteristics. Even though it enables the user to create stable virtual holograms in the real world, there has not yet been a systematic work to properly align the created virtual content with the world in a dynamic setting, which is required in many augmented reality applications. Although Vuforia SDK[1] has implemented image-tracking support on HoloLens, it does not completely address the alignment between virtual content and the user's view.

This paper takes a comprehensive approach to holographic OST-HMD calibration by devising a method, its implementation using various setups and trackers, experiment design and eventually a multimodal evaluation procedure. Furthermore, it provides an end-to-end solution for applications that require this type of display calibration.

In the following sections, we will first explain why existing

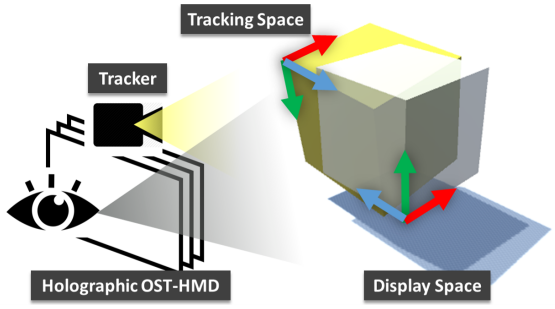

(a) Misalignment between the tracker space and holographic display space, example with head-anchored tracking system

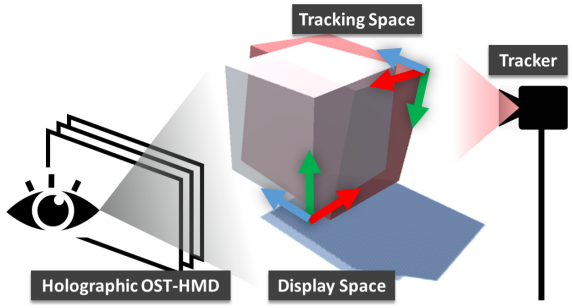

(b) Misalignment between the tracker space and holographic display space, example with world-anchored tracking system

Figure 1: Problem illustrated: If the holographic OST-HMD is not calibrated with the tracking system, the misalignment between them will cause uncomfortable augmented reality experience.

*L. Qian and E. Azimi contributed equally and are joint first authors.
†e-mail: long.qian@jhu.edu
‡e-mail: eazimi1@jhu.edu
§e-mail: pkaz@jhu.edu
¶e-mail: nassir.navab@tum.de

[1] https://vuforia.com/

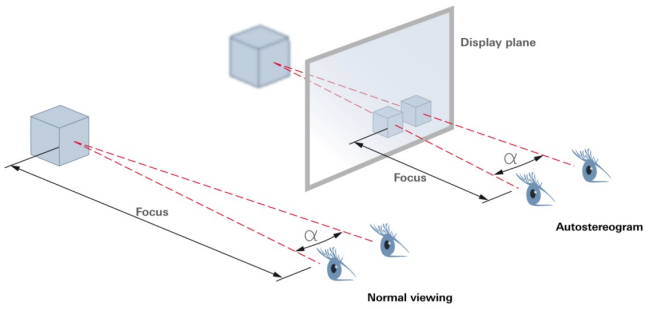

Figure 2: Difference between stereoscopic (right) and holographic scene generation (left) (image courtesy Reichelt et al. [28])

methods cannot appropriately be applied to holographic display calibration and why a new approach is necessary. Next, we incorporate the unique optical characteristics of the holographic display to find out the necessary equations for the calibration. Then, we describe the implementation of our calibration process and perform preliminary experiments using various trackers to perform the calibration. We evaluate our new method in two different ways, analyze the errors and validate its accuracy.

2 Background

2.1 Holographic Display

In order to properly calibrate an OST-HMD, it is necessary to have a calibration approach that can appropriately capture the optical characteristics of that specific OST-HMD [14]. There are different methods for generating 3D perception of the environment, which include stereoscopic and holographic techniques [24].

In stereoscopic displays, two different perspective views are generated almost simultaneously. The waves of light entering the eyes may have their origin on a common image plane which is generally fixed, as shown in Fig. 2 (right).

However, in holographic systems as illustrated in Fig. 2 (left), the waves of light forming the 3-D image may originate from different gaze-controlled image planes. The volumetric and the holographic approaches produce 3-D images where the effective origin of the waves entering the observer's eyes match with the apparent spatial position of the corresponding image points. Thus, holographic display systems mimic natural viewing for which there are distinct depth places that cover (in theory) the entire space [24]. Holographic display allows the reconstruction of natural looking 3-D scenes and creates a completely comfortable viewing experience for the user, while in almost all other 3-D stereo displays, there is eye strain due to depth cue mismatch of convergence and accommodation and other problems [28].

Based on the different inherent characteristics of 3D display techniques, existing techniques cannot be incorporated for the holographic head-mounted display; therefore, we need a different method that addresses these distinct characteristics.

2.2 OST-HMD Calibration

With optical see-through head-mounted display (OST-HMD) there is no direct access to the view of the users. Therefore, a user-dependent calibration procedure is generally required in order to correctly align the virtual content with its real counterpart. The Single Point Active Alignment Method (SPAAM) [30] is one of the widely applied methods to perform such display calibration due to its simplicity and accuracy. In SPAAM, 2D-3D point correspondences are collected by the user, and then a mapping from the 3D point cloud to its 2D screen coordinates is calculated using Direct Linear Transform (DLT) [13]. Methods have been proposed to improve the user interaction [12, 27] and robustness [3, 20] based on SPAAM. Unlike modeling the mapping from 3D point sets to the 2D screen coordinates as a projection, the DRC method [23] takes the physical model of the optics into account. Recently, interaction-free display calibration was developed with the help of an additional eye-tracking system [15, 16].

These methods calibrate one screen of the OST-HMD and one eye of the user. It is possible to perform the calibration procedure twice, in order for the rendered graphics on a stereoscopic OST-HMD to align correctly with the user's two eyes. Stereo-SPAAM [10] is a variant of SPAAM that simultaneously calibrates both eyes with a stereoscopic OST-HMD. Simultaneous calibration of stereoscopic OST-HMD is better conditioned by adding the physical constraints of two eyes, such as interpupillary distance (IPD) [26]. However, Stereo-SPAAM finds the projection matrix from the virtual camera formed by the eye to the planar screen; it merely calculates two separate 2D-3D mappings with the same underlying model.

Stepping from stereoscopic display into holographic display, the display volume for the user is no longer composed of two planar screens, but rather a full 3D perceptual space. The representation of information is therefore three-dimensional in space instead of two-dimensional within the screen coordinate system. As a consequence, the fundamental model of mapping becomes a 3D-3D registration procedure.

2.3 Tracking Systems

For a proper augmented reality application, virtuality should be perceptually registered with real objects during motion. A tracking system is able to provide the required geometry information of targeted objects in reality, so that the rendered graphics reflect the motion of them. Augmented reality based on head-mounted displays usually incorporates two categories of tracking system: head-anchored tracking system and world-anchored tracking system [31].

Many head-mounted display systems include an embedded front-facing camera, which can serve as the optical tracker for AR applications. Head-anchored tracking systems have the advantage of providing similar line of sight to that of the user, but its performance is limited by the size, power consumption, and computational cost. Calibration of OST-HMD using a head-mounted camera has been proposed [8, 11]. Marker-based tracking algorithms have the advantage in simplicity and robustness [9, 19], and marker-free tracking algorithms offer better user experience [18, 22].

In a world-anchored tracking system, the pose of the tracker coordinate system remains unchanged with respect to the world coordinate system. Without the constraints imposed by power, computational resources and the type of technology used, a world-anchored tracking system can potentially be accurate. Examples of world-anchored tracking systems include reflective markers tracker, electromagnetic sensing, and projective light-based tracker.

In this paper, calibration of holographic OST-HMD based on a head-anchored tracking system and a world-anchored tracking system are both studied and presented.

3 Method

In this section, we look into the OST-HMD calibration and projection matrix on a holographic display for the derivation of the required transformation.

We have a transform $T(\cdot)$ which maps 3D points from the world coordinates to a 3D virtual holographic environment. Basically, if we are given the points $q_1, \cdots, q_n$, through the transform we observe $p_1, \cdots, p_n$ such that

$$p_i = T(q_i) \quad i = 1, \cdots, n.$$

We assume that both p_i and $q_i \in \mathbb{R}^3$. The goal is to estimate T based on a set of observations in the form of (q_i, p_i) for $i = 1, \cdots, n$.

More specifically, the measurement of q_i is obtained from the tracking system, while the information of p_i is pre-defined and visualized on the holographic OST-HMD. With the calculated transform $T(\cdot)$, a point from the tracker coordinate system is mapped to that of the display coordinate system.

We further assume that the transformation $T(\cdot)$ is linear, and based on the linearity assumption, we solve for a general case where the transformation T is a perspective transformation, however an affine as well as an isometric transformation are also calculated to see how closely they can represent the result. Indeed, an affine or isometric transformation by having fewer unknown parameters can considerably reduce the burden and fatigue caused by performing several alignments for calibration. The mathematical representation of the three types are transformations are:

i) Perspective Transformation:

$$\hat{p}_i = \left[T_P\right]_{4\times4} \cdot \hat{q}_i, \quad T_P = \begin{bmatrix} p_{11} & p_{12} & p_{13} & p_{14} \\ p_{21} & p_{22} & p_{23} & p_{24} \\ p_{31} & p_{32} & p_{33} & p_{34} \\ p_{41} & p_{42} & p_{43} & p_{44} \end{bmatrix}$$

where both $\hat{p}_i$ and $\hat{q}_i$ are represented in **normalized** homogeneous coordinates, T_P is an arbitrary 4×4 matrix.

ii) Affine Transformation:

$$\hat{p}_i = \left[T_A\right]_{4\times4} \cdot \hat{q}_i, \quad T_A = \begin{bmatrix} a_{11} & a_{12} & a_{13} & a_{14} \\ a_{21} & a_{22} & a_{23} & a_{24} \\ a_{31} & a_{32} & a_{33} & a_{34} \\ 0 & 0 & 0 & 1 \end{bmatrix}$$

where the first three rows of T_A are arbitrary.

iii) Isometric Transformation:

$$\hat{p}_i = \left[T_I\right]_{4\times4} \cdot \hat{q}_i, \quad T_I = \begin{bmatrix} r_{11} & r_{12} & r_{13} & t_1 \\ r_{21} & r_{22} & r_{23} & t_2 \\ r_{31} & r_{32} & r_{33} & t_3 \\ 0 & 0 & 0 & 1 \end{bmatrix}$$

where T_I is composed of a 3×3 orthogonal matrix $\{r_{i,j}\}$ representing rotation, and a 3×1 translational vector $\vec{t}$.

With perspective transformation, 15 unknown parameters are calculated (excluding an arbitrary scale parameter), while affine transformation has 12 unknown parameters and isometric transformation has 6 unknown parameters. Both perspective transformation and affine transformation are calculated with the Direct Linear Transformation (DLT) algorithm, with the objective of minimizing total algebraic error [13]. For an isometric transformation, the problem is equal to registration of two rigid 3D point sets; therefore, the method of [1] is used, with the objective of minimizing least-square error of the registration.

The alignment task is performed by humans and is therefore prone to errors. The RANSAC [6] algorithm is used to find the most accurate transformation and reject any possible outliers based on the reprojection error of the samples. The average reprojection error of a certain transformation $T(\cdot)$ is represented as:

$$E_{reproj} = \frac{\sum_{i=1}^{n} \sqrt{(p_i - T(q_i))^2}}{n}$$

4 Implementation

We used Microsoft HoloLens (Microsoft Inc. USA) as the holographic OST-HMD. Due to the different characteristics of different tracking systems and to verify the applicability of our method, both head-anchored and world-anchored tracking systems were studied for the calibration.

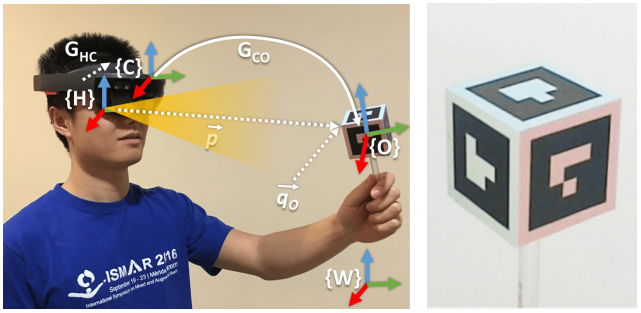

(a) Transformation graph (b) Tracked object

Figure 3: Implementation of the calibration with head-anchored tracking system. HoloLens embedded RGB camera is used as the head-anchored tracker. The transformation map of the calibration procedure is demonstrated. Fiducial markers are attached to different faces of the alignment object.

4.1 Calibration with Head-Anchored Tracking System

In this case, the embedded HoloLens front-facing RGB camera is used as the head-anchored optical tracker. Fiducial markers are attached to a real object that is held by the user. The coordinate systems of the tracker, object and holographic display are represented as $\{C\}$, $\{O\}$ and $\{H\}$ respectively. Since the camera is rigidly mounted on the holographic display itself, the extrinsic geometric transformation between the camera and the HoloLens G_{HC} is fixed. The point for alignment is fixed at $\vec{q_O}$ with respect to the coordinate system of $\{O\}$. Its corresponding virtual point is at $\vec{p}$ in the holographic display coordinate system $\{H\}$. The pose of the tracked object G_{CO} is determined with a marker-tracking package HoloLensARToolKit[2] at runtime. Eventually, the point sets $\{q \,|\, q_i = G_{CO,i} \cdot \vec{q_O}, i = 1, \cdots, n\}$ and $\{p_i \,|\, i = 1, \cdots, n\}$ are used for holographic OST-HMD calibration described in Section 3.

The package HoloLensARToolKit is based on ARToolKit [19], with extended compatibility with Windows Universal Platform (UWP), optimized functionalities for HoloLens, and integration with Unity3D[3]. HoloLensARToolKit is able to track matrix code markers, 2D pattern markers, and user-configured multi-markers. The HoloLens camera is calibrated using OpenCV[4]. When multiple markers are visible to the camera, the Iterative Closest Point (ICP) [5] algorithm helps to provide a robust tracking result. Fig. 3b is an example of a multi-marker object that is tracked by HoloLensARToolKit.

Along with this paper, the package HoloLensARToolKit is released open-source under LGPL v3 license[5], with the hope to help fellow researchers and engineers to build augmented reality applications on HoloLens that take advantage of the marker-tracking capabilities.

4.2 Calibration with World-Anchored Tracking System

The coordinate systems of the tracker, object, holographic display and world are represented as $\{E\}$, $\{O\}$, $\{H\}$ and $\{W\}$ respectively (Fig. 4a). The main conceptual difference between head-anchored and world-anchored tracking system for our calibration process is as follows.

In the head-mounted tracker case, the transformation G_{HC} between the tracker $\{C\}$ and the holographic display $\{H\}$ is fixed, but this is not the case for the world-anchored tracker, where the

[2] https://github.com/qian256/HoloLensARToolKit
[3] https://unity3d.com/
[4] http://opencv.org/
[5] https://www.gnu.org/licenses/lgpl-3.0.en.html

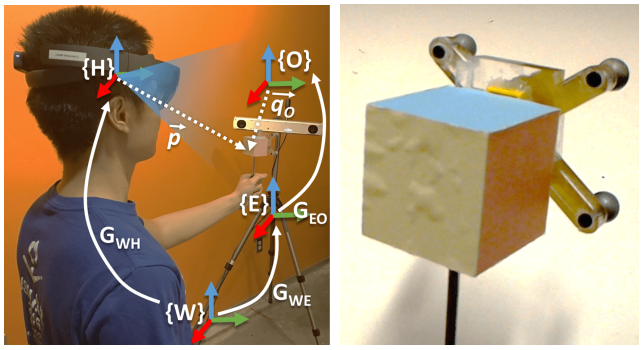

(a) Transformation graph (b) Tracked object

Figure 4: Implementation of the calibration with world-anchored tracking system. FusionTrack 500 is the world-anchored tracker. Passive spherical markers form a frame that is attached to the colored cube for tracking.

transformation G_{HE} is expressed as $G_{HE} = {G_{WH}}^{-1} \cdot G_{WE}$. Since the world-anchored tracker does not change its pose in the room, G_{WE} is fixed. Therefore, an extra component is needed to maintain and update the transformation G_{WH} between the world and holographic display $\{H\}$, so that the transformation between the tracker and the display G_{HE} can be determined. The SLAM-based spatial mapping capability of the HoloLens fills this gap and completes our transformation chain from the tracked object to the user's view. For HMDs that do not perform spatial mapping, another method would be required, such as using the external tracking system to also track the HMD. In fact, to the best of our knowledge, this is the first time that the self localization and spatial mapping of a HMD is used for the calibration where no line of sight is required between the HMD and tracking system or tracked object.

In our implementation for the world-anchored tracker experiment, we used a FusionTrack 500 (Atracsys, Switzerland). Passive spherical markers compose a frame which is attached to the cube that is used for alignment (Fig. 4b). A component is written in C++ to handle processing and transmission for the external tracker. Tracking information of the tracked objects is obtained with frequency of over 300 Hz and is transmitted to the HoloLens via a wireless network. The UDP protocol was used to minimize latency and allow real-time performance.

5 Experiment

To analyze and evaluate our proposed calibration method, experiments were designed as follows. The experiments are carried out with the two different types of trackers followed by their evaluation. The overall workflow diagrams for the calibration with head-anchored tracker and world-anchored tracker are depicted in Fig. 5.

5.1 Experimental setup

As explained in Section 3, we used two different types of tracking systems for our method to be more general and cover a wider range of potential applications. For the same reason, two different experiment setups were designed to represent both tracker types.

Fig. 3a represents our experiment setup for the head-anchored tracker case. To perform the alignment easier in a holographic display and provide a better depth cue in this procedure, we needed a 3D object rather than the 2D crosshair that is typically used for SPAAM or the planar disk used for Stereo-SPAAM [10]. Thus, we used a $2'' \times 2'' \times 2''$ cube with different fiducial markers attached on its faces and painted each face with a different color that matches its counterpart in the holographic cube, as shown in Fig. 3b, to make the alignment task even easier.

Fig. 4a represents our experiment setup for use with the world-anchored tracker. In this case, we attached our passive markers with reflective spheres to the painted cube (Fig. 4b) and since the alignment is done relative to the cube, a pivot calibration was performed to obtain the transformation from the tracked passive markers to the attached cube.

The general calibration procedure does not differ from one tracker to another and is explained as follows. First, as represented in Figs. 3a and 4a, the user wears the holographic OST-HMD and is given a real object for alignment. Before calibration, the virtual overlay is not correctly aligned with the tracked cube, as shown in Figs. 6a and 7a. Using automated voice commands, s/he is then instructed to perform the calibration step by step. First, a virtual cube is displayed and the user should try to align only one corner of the cube with its real counterpart in her/his hand (Figs. 6b and 7b). Once s/he is satisfied with the alignment, a button is clicked for the confirmation. It should be noted that only the corner position is measured for the alignment, however the holographic scene also illustrates a cube with colored faces that matches the real cube. This makes the alignment task more intuitive with the additional depth cue and color similarity. Next, the virtual cube appears in another location in the user's field of view. We try to cover the entire workspace within the reach of the user so that our calibration results are balanced and less biased towards a certain geometrical location. This process continues until 20 points are collected, when the system informs the user of the conclusion of the calibration. At this point the perspective, affine and isometric 3D projection matrices are calculated with their corresponding reprojection error. The user is able to select from the transformations with different geometrical models, and see the virtual cube in the holographic environment superimposed on the real cube (Figs. 6c and 7c).

5.2 Evaluation

Evaluating an OST-HMD calibration has always been challenging since only the user wearing it can observe the superimposed objects that resulted from the calibration. In order to make this process more objective, some studies used a camera instead of the user's eye [20] and did their measurements from the images captured by that "eye camera." However, in our case as explained in Section 2.1, the display system is inherently 3D and using a camera will inevitably remove the depth information, which is a distinctive dimension for the holographic display. Moreover, using a camera would necessitate that the accuracy be reported in dimensionless pixels, while both our world and holographic coordinate systems are using metric Cartesian dimensions for which there is a generic understanding across the community. In other words, it will have significantly different implications for two calibrations that both have 5 pixels reprojection error along an axis, if that error is equivalent to 5 millimeters or 50 centimeters in the real world. Two evaluation methods are devised to better analyze the accuracy of our proposed calibration.

i) Train-and-Test:

In the first evaluation method, we used an approach similar to part of the study done by Itoh et al. [15], in which a train-and-test scheme is used. Specifically, the user is asked to collect 8 additional samples, and these samples are tested against the calibration calculated with the training data sets consisting of the 20 alignments. Reprojection error of the test data is computed based on each of the three transformation matrices (perspective, affine, isometric).

ii) Double-Cube-Match:

In the second evaluation analysis, a second cube marker is used as an auxiliary reference for objective measurement of the calibration error.

Using the computed transformation from the calibration phase, a virtual cube is displayed in the holographic scene with a predetermined offset of 150 mm with respect to the first marker cube at four

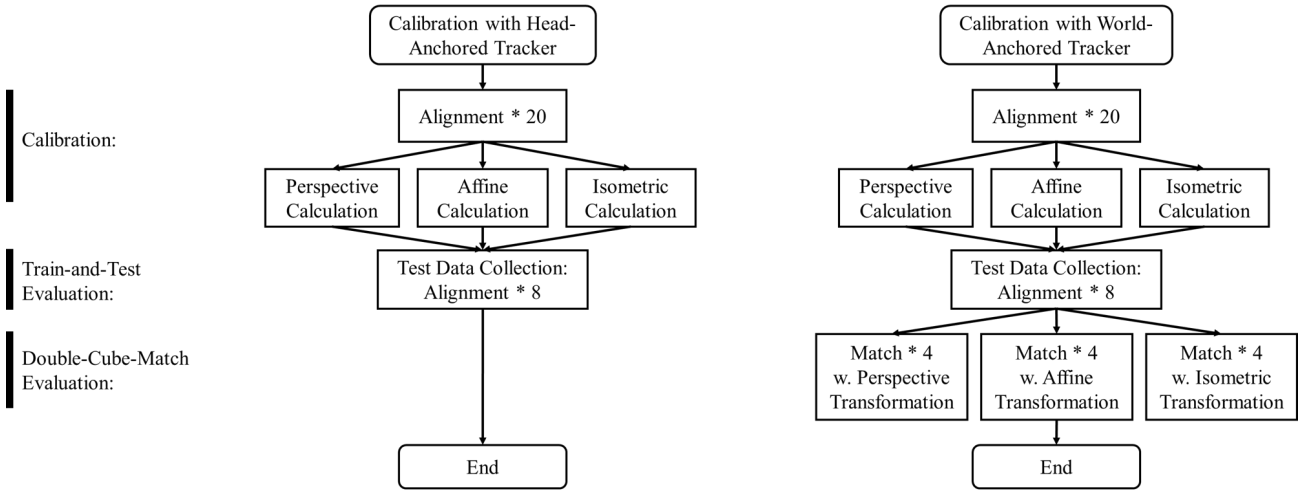

Figure 5: The workflow of calibration with head-anchored tracker and world-anchored tracker

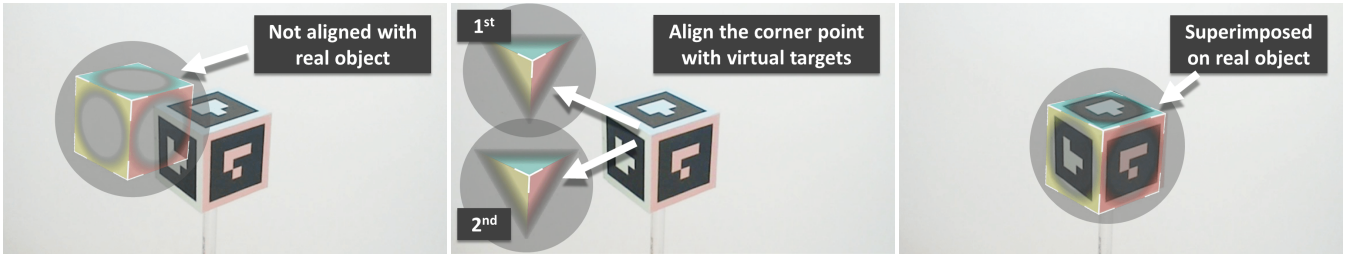

(a) See-through view before calibration (b) Alignment process with automated voice instructions (c) Superimposed cube after calibration

Figure 6: Calibration process using head-anchored tracker

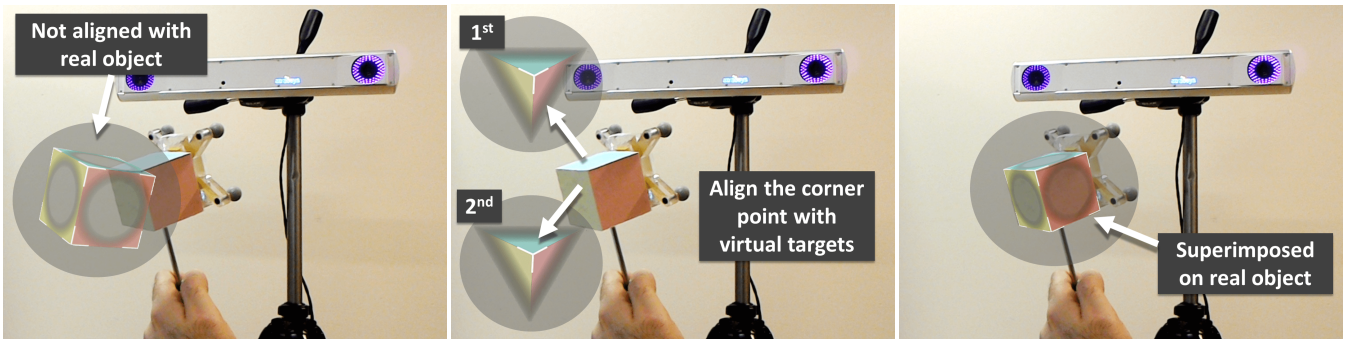

(a) See-through view before calibration (b) Alignment process with automated voice instructions (c) Superimposed cube after calibration

Figure 7: Calibration process using world-anchored tracker

different equidistant positions. The user is now asked to align the second real marker cube with the displayed virtual cube as precisely as possible by moving it relative to the other. There are three major sources of error contributing to our observation from this evaluation. In addition to errors generated in the calibration process that we are seeking, there is also error that can be caused by poor alignment. Another error is due to uncertainties in the self localization system of the HMD. To minimize the effect of poor alignment and also eliminate the effects of hand tremor on the alignment in the evaluation process, the tracked cubes are mounted on a flexible stand as shown in 8. Since with this setup, it is no longer necessary to keep the cube in the user's hand, it also allows the user to move around the target and verify the proper alignment from different viewpoints, where distances from the object are no longer limited by the user's arm length. When s/he is satisfied with the alignment, a button is pressed on the keyboard to record the positions of the markers at that instant. The difference between the predetermined offset pose and the observed object pose at the point of the user's confirmation is used as the metric to evaluate the accuracy of the calibration. One might argue that the alignment is still reported by the user, but we assume that as long as the measurements are done by an independent observer (accurate tracking system) to which the user is blind, it serves well for the scope of optical see-through calibration from the perspective of the end user.

The reported metric in this developed evaluation should be representative of the whole transformation yet intuitive enough that it

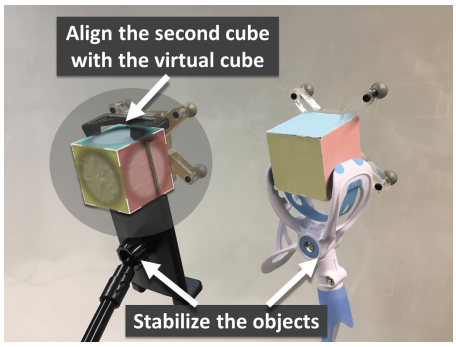

(a) View of the first cube and its hologram with a 150 mm offset before the alignment

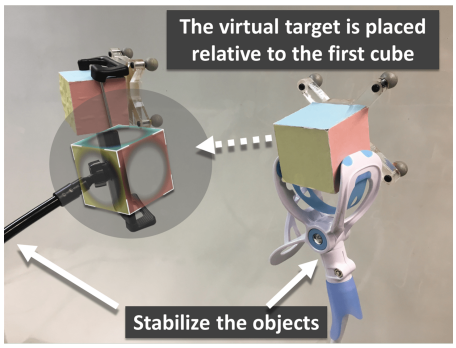

(b) Display after the alignment of the second tracked cube with the first generated hologram

Figure 8: Evaluation process using external measurement system

can be analyzed with similar systems. Therefore, average displacement error $E_{\Delta p}$ as well as average rotation error using quaternion representation $E_{\Delta q}$ following the method described in [21] are calculated for error analysis where:

$$E_{\Delta p} = \frac{\sum_{i=1}^{n} \sqrt{(\Delta p_{Measured} - \Delta p_{Desired})^2}}{n}$$

and average quaternion is obtained by:

$$\tilde{q} = \arg\max_{q \in \mathbb{S}^3} q^T M q$$

Where, $q = (w, x, y, z)$, S^3 denotes the unit 3-sphere, and M is a 4×4 matrix derived from quaternions [21].

6 Results and Discussion

The graphical representation of the tracked calibrated cube with its virtual counterpart in a holographic head-mounted display is illustrated in 6c and 7c, against the non-calibrated ones 6a and 7a. It can be seen that the calibrated one is well aligned, while the uncalibrated one is visibly misaligned. The calibration process was able to superimpose the holographic cube in the correct pose with regard to its real tracked counterpart.

Two users familiar with various HMD systems and calibration techniques performed the calibration with each tracking system in 10 trials followed by the corresponding evaluations. The results and error analysis is presented here:

Calibration with Head-Anchored Tracker:

The train-and-test evaluation method is applied to the calibration with the head-anchored tracker, for the three different geometrical models. In each calibration trial (20 trials in total), 20 alignments are used for training, and 8 alignments are used for testing purposes.

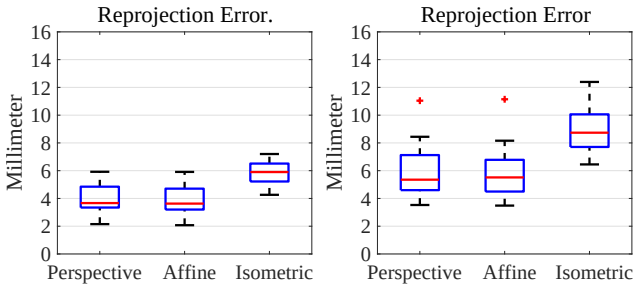

(a) Calib. with head-anchored tracker (b) Calib. with world-anchored tracker

Figure 9: Evaluation result of Train-and-Test for the calibration with head-anchored tracker and world-anchored tracker, based on different geometrical models.

At the training stage, the mean and standard deviation of the residue of each geometrical model are shown: perspective transformation ($3.10 \pm 0.98mm$), affine transformation ($3.24 \pm 1.02mm$), and isometric transformation ($5.55 \pm 0.67mm$). One alignment is identified as an outlier and excluded at this stage. As expected, the training residue decreases in the same order with respect to the number of parameters in the geometrical model.

Fig. 9a represents the reprojection error of the testing data using perspective, affine and isometric transformation matrices. The mean and standard deviation of the reprojection error are: perspective ($4.04 \pm 1.04mm$), affine ($3.96 \pm 1.06mm$), and isometric ($5.86 \pm 0.81mm$). A closer look into the results indicates that both affine and perspective transformations generated 3D holographic overlays with reasonable accuracy ($\sim 4mm$) but the isometric transformation had a couple of mm more error for the internal tracking case. At both training and testing stages, the performance of the perspective and affine models are similar, and are both moderately better than the isometric model. In this case, the affine model is the most suitable representation of the transformation between the space of the tracker and the frame of the holographic display with reduced number of unknowns. In other words, the loss of precision of the affine transformation is negligible compared to the perspective one with fewer number of alignments.

Table 1: Reprojection error along different axes for the calibration with head-anchored tracking system

Model	Axis X (mm)		Axis Y (mm)		Axis Z (mm)	
	mean	std	mean	std	mean	std
Perspective	1.00	0.81	0.91	0.68	3.55	2.62
Affine	0.94	0.74	0.83	0.63	3.51	2.67
Isometric	1.82	1.08	2.05	1.36	4.58	3.31

Table 1 shows the mean and standard deviation of the reprojection error along different axes with different geometrical models. Here, the xy plane is perpendicular to the user's view, and the z axis is parallel with the user's line of sight, indicating the depth of alignment. The results show that the error of the alignment in depth is still largest among the three directions, for all geometrical models. Depth alignment is difficult because the visual appearance of varied depth is not as salient as that of the xy plane. In addition, considering our tracking system, marker-based *inside-out* optical tracking studies also show that the tracking result is most vulnerable along the depth direction [4, 7]. However, efforts have been made to utilize the depth cue of the holographic display to provide a better depth perception for the users, and at least the magnitude of error along the depth axis is successfully kept almost the same.

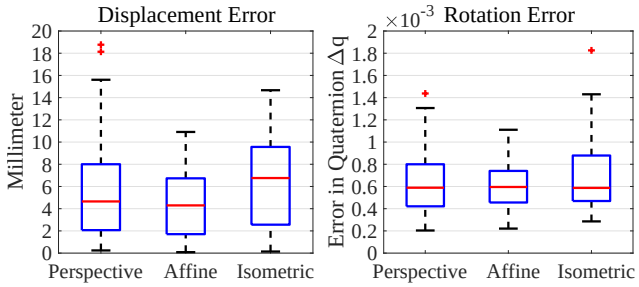

(a) Displacement error $E_{\Delta P}$

(b) Rotational error $E_{|\Delta q|}$

Figure 10: Evaluation result of Double-Cube-Match for the calibration with world-anchored tracker. After the calibration, the user was able to align the pose of the cube with high accuracy

The geometrical models proposed in this paper are all linear models, that is to say, the calibration only covers the linear transformation between the display coordinate system and the tracking coordinate system. Therefore, the linearity assumption implicitly poses an additional requirement on the tracking system that is being used. In this example, the front-facing RGB camera of HoloLens needs to be calibrated well, so that the distortion of the image can be handled while tracking.

Calibration with World-Anchored Tracker:

Both Train-and-Test and Double-Cube-Match metrics are used to evaluate the calibration with the world-anchored tracking system.

Train-and-Test evaluation of the calibration with the world-anchored tracker is similar to that of the head-anchored tracker. The residue at the training stage is listed as follows: perspective transformation ($3.90 \pm 0.82mm$), affine transformation ($4.03 \pm 0.87mm$), and isometric transformation ($9.93 \pm 1.47mm$). One alignment outlier is identified and excluded.

The reprojection error of the calibration results applied on the testing dataset is shown in Fig. 9b. For perspective transformation, the mean and standard deviation of reprojection error is $5.88 \pm 1.81mm$, while affine transformation yields an error of $5.83 \pm 1.78mm$, and isometric transformation yields an error of $8.92 \pm 1.60mm$.

Table 2: Reprojection error along different axes for the calibration with world-anchored tracking system

Model	Axis X (mm)		Axis Y (mm)		Axis Z (mm)	
	mean	std	mean	std	mean	std
Perspective	2.47	2.04	3.01	2.49	3.20	3.01
Affine	2.44	1.98	2.98	2.52	3.21	3.01
Isometric	3.64	2.75	6.14	3.88	3.43	2.93

Table 2 demonstrates the distribution of error along different axes. However, in the case of calibration with the world-anchored tracker, the x, y, and z axis are parallel to the world coordinate system $\{W\}$. The user is able to move around and make alignments from different viewing perspectives. Therefore, no axis is associated with the depth direction in this case, as indicated from the error values.

Fig. 10 depicts the evaluation results of the Double-Cube-Match metric. Fig. 10a shows the distribution of displacement with the three different models. More specifically, for perspective transformation, the displacement error is $5.47 \pm 4.26mm$; for affine transformation, the displacement error is $4.45 \pm 3.00mm$, and for isometric transformation, the displacement error is $6.44 \pm 4.15mm$.

Analysis of a transformation without a thorough look at the orientation is not complete. Therefore, errors in the orientation in Double-Cube-Match were measured and represented in 10b. Excluding a couple of outliers for the isometric case, the user was able to match the orientation of cubes with a very high accuracy using all calibration matrices. The average error in quaternion for the affine transformation $E_{\Delta q}$ is given by $(0.999, 0.005, 0.002, 0.007)$ where q follows $q = (w, x, y, z)$ representation. Similarly, for the perspective transformation, the quaternion error is $(0.999, 0.001, 0.001, 0.001)$ and $(0.999, 0.009, 0.002, 0.003)$ for the isometric transformation. This excellent accuracy in orientation can be attributed to the fact that the entire virtual cube is visualized in Double-Cube-Match; and the user can take multiple viewpoints to adjust the orientation of the real cube using the color similarity and achieve a very accurate alignment.

From both evaluation methods, one can observe that the affine model captures the transformation from the Atracsys tracker to the HoloLens display better than both the perspective model and the isometric model.

It should also be noted that tracking volumes for these two setups are different. For the head-anchored tracking system, the calibration volume is a frustum (close plane: $110.88cm^2$, far plane: $38.88cm^2$, depth range: $12cm$) due to the limit of field-of-view of HoloLens and the user's arm reach. The world-anchored tracking system covers a larger volume ($60cm \times 60cm \times 60cm$). Therefore, the amount of errors should be analyzed in its own context.

In addition, we are not able to compare the accuracy and precision of the proposed calibration method with other techniques such as SPAAM or Stereo-SPAAM which are typically used for conventional OST-HMD calibration. As it was discussed in 2.1, holographic and non-holographic HMDs have fundamental differences in their optics and projection system and one calibration method cannot essentially be applied to the other system and vice versa.

7 Future Work

In the future, we aim to integrate head-anchored and world-anchored tracking systems in the holographic OST-HMD using sensor fusion, thereby overcoming issues such as occlusion or limited field of view.

Currently, 20 point correspondences are collected to allow us to study the geometrical models of the calibration of the holographic OST-HMD from a scientific point of view; however, the theoretical minimum number of alignments is only 5 for perspective transformation, and even fewer for isometric and affine transformations. In order to improve the user experience in such a calibration procedure, we will implement a user-friendly, intuitive and easy task for calibration. A full user study will be conducted to look into issues such as fatigue and user-friendliness of the proposed method.

Additionally, we will try to use our holographic OST-HMD calibration for tasks involving tool tracking and navigation in a mixed reality setting.

8 Conclusion

Existing calibration methods cannot be utilized for holographic OST-HMD systems. In the present study, we proposed a method for calibration of holographic head-mounted displays using various tracking systems using perspective, affine and isometric transformation models. Experimental results indicated that the accuracy of our calibration was up to 4 mm in terms of the average reprojection error and our more objective evaluation indicated that the average displacement error was almost 4 mm as well.

In addition, in a novel approach we successfully incorporated the self localization and spatial mapping of an OST-HMD in a calibration process, thereby eliminating the need for a line of sight from the HMD to the tracker or object.

Furthermore, to address the challenge of subjectivity in evaluation of OST-HMDs, a new evaluation method, namely Double-Cube-Match, was proposed which is less subjective and incorporates an external measurement system as an independent observer.

ACKNOWLEDGEMENTS

This work was supported in part by the US Army Medical Research and Materiel Command under Contract W81XWH-15-C-0156, awarded to Juxtopia LLC. The contents should not be construed as an official Department of the Army position, policy or decision unless so designated by other documentation.

REFERENCES

[1] K. S. Arun, T. S. Huang, and S. D. Blostein. Least-squares fitting of two 3-D point sets. *IEEE Transactions on Pattern Analysis and Machine Intelligence*, 9(5):698–700, 1987.

[2] E. Azimi, J. Doswell, and P. Kazanzides. Augmented reality goggles with an integrated tracking system for navigation in neurosurgery. In *Virtual Reality Short Papers and Posters (VRW)*, pages 123–124. IEEE, 2012.

[3] E. Azimi, L. Qian, P. Kazanzides, and N. Navab. Robust optical see-through head-mounted display calibration: Taking anisotropic nature of user interaction errors into account. In *Virtual Reality (VR)*. IEEE, 2017.

[4] M. Bauer. *Tracking errors in augmented reality.* PhD thesis, Technical University Munich, 2007.

[5] P. J. Besl and N. D. McKay. Method for registration of 3-D shapes. *IEEE Trans. on Pattern Analysis and Machine Intelligence*, 14(2):239–256, 1992.

[6] M. A. Fischler and R. C. Bolles. Random sample consensus: a paradigm for model fitting with applications to image analysis and automated cartography. *Communications of the ACM*, 24(6):381–395, 1981.

[7] R. M. Freeman, S. J. Julier, and A. J. Steed. A method for predicting marker tracking error. In *6th IEEE/ACM International Symposium on Mixed and Augmented Reality (ISMAR)*, pages 157–160. IEEE, 2007.

[8] A. Fuhrmann, D. Schmalstieg, and W. Purgathofer. Practical calibration procedures for augmented reality. In *Virtual Environments 2000*, pages 3–12. Springer, 2000.

[9] S. Garrido-Jurado, R. Muñoz-Salinas, F. J. Madrid-Cuevas, and M. J. Marín-Jiménez. Automatic generation and detection of highly reliable fiducial markers under occlusion. *Pattern Recognition*, 47(6):2280–2292, 2014.

[10] Y. Genc, F. Sauer, F. Wenzel, M. Tuceryan, and N. Navab. Optical see-through HMD calibration: A stereo method validated with a video see-through system. In *IEEE/ACM International Symposium on Augmented Reality (ISAR)*, pages 165–174. IEEE, 2000.

[11] Y. Genc, M. Tuceryan, A. Khamene, and N. Navab. Optical see-through calibration with vision-based trackers: Propagation of projection matrices. In *IEEE/ACM International Symposium on Augmented Reality (ISAR)*, pages 147–156. IEEE, 2001.

[12] Y. Genc, M. Tuceryan, and N. Navab. Practical solutions for calibration of optical see-through devices. In *1st International Symposium on Mixed and Augmented Reality (ISMAR)*, page 169. IEEE Computer Society, 2002.

[13] R. Hartley and A. Zisserman. *Multiple view geometry in computer vision*. Cambridge University Press, 2003.

[14] Y. Itoh, T. Amano, D. Iwai, and G. Klinker. Gaussian light field: Estimation of viewpoint-dependent blur for optical see-through head-mounted displays. *IEEE Transactions on Visualization and Computer Graphics*, 22(11):2368–2376, 2016.

[15] Y. Itoh and G. Klinker. Interaction-free calibration for optical see-through head-mounted displays based on 3d eye localization. In *IEEE Symposium on 3D User Interfaces (3DUI)*, pages 75–82. IEEE, 2014.

[16] Y. Itoh and G. Klinker. Performance and sensitivity analysis of indica: Interaction-free display calibration for optical see-through head-mounted displays. In *IEEE International Symposium on Mixed and Augmented Reality (ISMAR)*, pages 171–176. IEEE, 2014.

[17] A. L. Janin, D. W. Mizell, and T. P. Caudell. Calibration of head-mounted displays for augmented reality applications. In *Virtual Reality Annual International Symposium*, pages 246–255. IEEE, 1993.

[18] D. Joseph Tan, F. Tombari, S. Ilic, and N. Navab. A versatile learning-based 3d temporal tracker: Scalable, robust, online. In *Proceedings of the IEEE International Conference on Computer Vision*, pages 693–701, 2015.

[19] H. Kato and M. Billinghurst. Marker tracking and HMD calibration for a video-based augmented reality conferencing system. In *2nd IEEE/ACM International Workshop on Augmented Reality (IWAR)*, pages 85–94. IEEE, 1999.

[20] N. Makibuchi, H. Kato, and A. Yoneyama. Vision-based robust calibration for optical see-through head-mounted displays. In *20th IEEE International Conference on Image Processing (ICIP)*, pages 2177–2181. IEEE, 2013.

[21] F. L. Markley, Y. Cheng, J. L. Crassidis, and Y. Oshman. Averaging quaternions. *Journal of Guidance, Control, and Dynamics*, 30(4):1193–1197, 2007.

[22] R. A. Newcombe, S. Izadi, O. Hilliges, D. Molyneaux, D. Kim, A. J. Davison, P. Kohi, J. Shotton, S. Hodges, and A. Fitzgibbon. Kinectfusion: Real-time dense surface mapping and tracking. In *10th IEEE International Symposium on Mixed and Augmented Reality (ISMAR)*, pages 127–136. IEEE, 2011.

[23] C. B. Owen, J. Zhou, A. Tang, and F. Xiao. Display-relative calibration for optical see-through head-mounted displays. In *Third IEEE and ACM International Symposium on Mixed and Augmented Reality (ISMAR)*, pages 70–78. IEEE, 2004.

[24] S. Pastoor and M. Wöpking. 3-d displays: A review of current technologies. *Displays*, 17(2):100–110, 1997.

[25] L. Qian, A. Barthel, A. Johnson, G. Osgood, P. Kazanzides, N. Navab, and B. Fuerst. Comparison of optical see-through head-mounted displays for surgical interventions with object-anchored 2d-display. *International Journal of Computer Assisted Radiology and Surgery*, 2017.

[26] L. Qian, A. Winkler, B. Fuerst, P. Kazanzides, and N. Navab. Modeling physical structure as additional constraints for stereoscopic optical see-through head-mounted display calibration. In *IEEE International Symposium on Mixed and Augmented Reality (ISMAR-Adjunct)*, pages 154–155. IEEE, 2016.

[27] L. Qian, A. Winkler, B. Fuerst, P. Kazanzides, and N. Navab. Reduction of interaction space in single point active alignment method for optical see-through head-mounted display calibration. In *IEEE International Symposium on Mixed and Augmented Reality (ISMAR-Adjunct)*, pages 156–157. IEEE, 2016.

[28] S. Reichelt, A. Schwerdtner, G. Futterer, H. Stolle, N. Leister, and R. Haussler. *Holographic 3-D displays-electro-holography within the grasp of commercialization*. INTECH Open Access Publisher, 2010.

[29] P. Sadda, E. Azimi, G. Jallo, J. Doswell, and P. Kazanzides. Surgical navigation with a head-mounted tracking system and display. *Studies in Health Technology and Informatics*, 184:363–369, 2012.

[30] M. Tuceryan, Y. Genc, and N. Navab. Single-point active alignment method (SPAAM) for optical see-through HMD calibration for augmented reality. *Presence: Teleoperators and Virtual Environments*, 11(3):259–276, 2002.

[31] J. Wang, L. Qian, E. Azimi, and P. Kazanzides. Prioritization and static error compensation for multi-camera collaborative tracking in augmented reality. In *Virtual Reality (VR)*. IEEE, 2017.